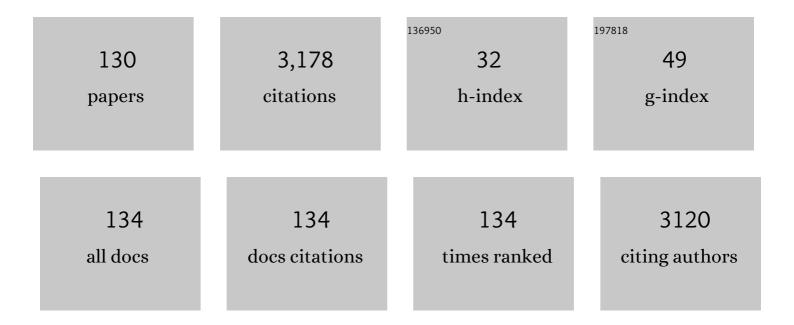
List of Publications by Year in descending order

Source: https://exaly.com/author-pdf/6851436/publications.pdf Version: 2024-02-01



ΗλΝΙΙΙΙΙ

#	Article	IF	CITATIONS
1	EEG phase-amplitude coupling to stratify encephalopathy severity in the developing brain. Computer Methods and Programs in Biomedicine, 2022, 214, 106593.	4.7	6
2	Photobiomodulation at Different Wavelengths Boosts Mitochondrial Redox Metabolism and Hemoglobin Oxygenation: Lasers vs. Light-Emitting Diodes In Vivo. Metabolites, 2022, 12, 103.	2.9	17
3	Metabolic Connectivity and Hemodynamic-Metabolic Coherence of Human Prefrontal Cortex at Rest and Post Photobiomodulation Assessed by Dual-Channel Broadband NIRS. Metabolites, 2022, 12, 42.	2.9	10
4	Combination of Group Singular Value Decomposition and eLORETA Identifies Human EEG Networks and Responses to Transcranial Photobiomodulation. Frontiers in Human Neuroscience, 2022, 16, .	2.0	9
5	Feasibility of EEG Phase-Amplitude Coupling to Stratify Encephalopathy Severity in Neonatal HIE Using Short Time Window. Brain Sciences, 2022, 12, 854.	2.3	3
6	Alterted Adipogenesis of Human Mesenchymal Stem Cells by Photobiomodulation Using 1064 nm Laser Light. Lasers in Surgery and Medicine, 2021, 53, 263-274.	2.1	6
7	Regional heterogeneity of cerebral hemodynamics in mild neonatal encephalopathy measured with multichannel near-infrared spectroscopy. Pediatric Research, 2021, 89, 882-888.	2.3	5
8	Preclinical studies of transcranial photobiomodulation in the neurological diseases. Translational Biophotonics, 2021, 3, e202000024.	2.7	3
9	Neurovascular coupling (NVC) in newborns using processed EEG versus amplitude-EEG. Scientific Reports, 2021, 11, 9426.	3.3	9
10	EEG Spectral Power: A Proposed Physiological Biomarker to Classify the Hypoxic-Ischemic Encephalopathy Severity in Real Time. Pediatric Neurology, 2021, 122, 7-14.	2.1	8
11	Transcranial photobiomodulation and thermal stimulation induce distinct topographies of EEG alpha and beta power changes in healthy humans. Scientific Reports, 2021, 11, 18917.	3.3	26
12	Dependance of variance in estimation of hemoglobin concentration changes on system noise and two wavelengths chosen. , 2021, , .		0
13	Wavelet-based neurovascular coupling can predict brain abnormalities in neonatal encephalopathy. NeuroImage: Clinical, 2021, 32, 102856.	2.7	13
14	A recursive partitioning approach for subgroup identification in brain–behaviour correlation analysis. Pattern Analysis and Applications, 2020, 23, 161-177.	4.6	2
15	Learning Hemodynamic Effect of Transcranial Infrared Laser Stimulation Using Longitudinal Data Analysis. IEEE Journal of Biomedical and Health Informatics, 2020, 24, 1772-1779.	6.3	11
16	Transcranial Photobiomodulation (tPBM) With 1,064â€nm Laser to Improve Cerebral Metabolism of the Human Brain In Vivo. Lasers in Surgery and Medicine, 2020, 52, 807-813.	2.1	34
17	Differences in Net Information Flow and Dynamic Connectivity Metrics Between Physically Active and Inactive Subjects Measured by Functional Near-Infrared Spectroscopy (fNIRS) During a Fatiguing Handgrip Task. Frontiers in Neuroscience, 2020, 14, 167.	2.8	13
18	Alterations of Cerebral Hemodynamics and Network Properties Induced by Newsvendor Problem in the Human Prefrontal Cortex. Frontiers in Human Neuroscience, 2020, 14, 598502.	2.0	6

#	Article	IF	CITATIONS
19	Transcranial photobiomodulation-induced changes in human brain functional connectivity and network metrics mapped by whole-head functional near-infrared spectroscopy in vivo. Biomedical Optics Express, 2020, 11, 5783.	2.9	21
20	Functional connectivity changes from transcranial infrared laser stimulation measured by functional near-infrared spectroscopy. , 2020, , .		0
21	Topography of alpha rhythms evoked by transcranial laser neuromodulation and thermal stimulation. , 2020, , .		0
22	Cognitive Enhancement by Transcranial Photobiomodulation Is Associated With Cerebrovascular Oxygenation of the Prefrontal Cortex. Frontiers in Neuroscience, 2019, 13, 1129.	2.8	40
23	Anticipatory alpha oscillation predicts attentional selection and hemodynamic response. Human Brain Mapping, 2019, 40, 3606-3619.	3.6	28
24	Commentaries on Viewpoint: Managing the power grid: How myoglobin can regulate Po2 and energy distribution in skeletal muscle. Journal of Applied Physiology, 2019, 126, 791-794.	2.5	2
25	Transcranial photobiomodulation with 1064-nm laser modulates brain electroencephalogram rhythms. Neurophotonics, 2019, 6, 1.	3.3	40
26	Mapping cortical network effects of fatigue during a handgrip task by functional near-infrared spectroscopy in physically active and inactive subjects. Neurophotonics, 2019, 6, 1.	3.3	17
27	Characterization of the functional nearâ€infrared spectroscopy response to nociception in a pediatric population. Paediatric Anaesthesia, 2018, 28, 103-111.	1.1	5
28	Cortical activity in fineâ€motor tasks in children with Developmental Coordination Disorder: A preliminary fNIRS study. International Journal of Developmental Neuroscience, 2018, 65, 83-90.	1.6	27
29	Exploring brain functional connectivity in rest and sleep states: a fNIRS study. Scientific Reports, 2018, 8, 16144.	3.3	45
30	Concurrent measurement of skeletal muscle blood flow during exercise with diffuse correlation spectroscopy and Doppler ultrasound. Biomedical Optics Express, 2018, 9, 131.	2.9	15
31	Modulating the resting-state functional connectivity patterns of language processing areas in the human brain with anodal transcranial direct current stimulation applied over the Broca's area. Neurophotonics, 2018, 5, 1.	3.3	11
32	Whole-cortical graphical networks at wakeful rest in young and older adults revealed by functional near-infrared spectroscopy. Neurophotonics, 2018, 5, 1.	3.3	13
33	Directional changes in information flow between human brain cortical regions after application of anodal transcranial direct current stimulation (tDCS) over Broca's area. Biomedical Optics Express, 2018, 9, 5296.	2.9	21
34	Elevated cranial ultrasound resistive indices are associated with improved neurodevelopmental outcomes one year after pediatric cardiac surgery: A single center pilot study. Heart and Lung: Journal of Acute and Critical Care, 2017, 46, 251-257.	1.6	8
35	Up-regulation of cerebral cytochrome-c-oxidase and hemodynamics by transcranial infrared laser stimulation: A broadband near-infrared spectroscopy study. Journal of Cerebral Blood Flow and Metabolism, 2017, 37, 3789-3802.	4.3	133
36	Diffuse correlation spectroscopy (DCS) study of blood flow changes during low level laser therapy (LLLT): a preliminary report. , 2017, , .		1

#	Article	IF	CITATIONS
37	Are there gender differences in young vs. aging brains under risk decision-making? An optical brain imaging study. Brain Imaging and Behavior, 2017, 11, 1085-1098.	2.1	21
38	Impairment of cerebral autoregulation in pediatric extracorporeal membrane oxygenation associated with neuroimaging abnormalities. Neurophotonics, 2017, 4, 1.	3.3	23
39	Impact of heat on metabolic and hemodynamic changes in transcranial infrared laser stimulation measured by broadband near-infrared spectroscopy. Neurophotonics, 2017, 5, 1.	3.3	52
40	On the optimization of imaging protocol for the mapping of cerebrovascular reactivity. Journal of Magnetic Resonance Imaging, 2016, 43, 661-668.	3.4	17
41	Prefrontal hemodynamic mapping by functional near-infrared spectroscopy in response to thermal stimulations over three body sites. Neurophotonics, 2016, 3, 045008.	3.3	16
42	Is EEG causal to fNIRs?. , 2016, , .		2
43	Interplay between up-regulation of cytochrome-c-oxidase and hemoglobin oxygenation induced by near-infrared laser. Scientific Reports, 2016, 6, 30540.	3.3	144
44	Simultaneous multiâ€ s lice (SMS) acquisition enhances the sensitivity of hemodynamic mapping using gas challenges. NMR in Biomedicine, 2016, 29, 1511-1518.	2.8	9
45	Transcranial laser stimulation improves human cerebral oxygenation. Lasers in Surgery and Medicine, 2016, 48, 343-349.	2.1	116
46	Automated voxel classification used with atlas-guided diffuse optical tomography for assessment of functional brain networks in young and older adults. Neurophotonics, 2016, 3, 045002.	3.3	10
47	Dimensionality Reduction Based Optimization Algorithm for Sparse 3-D Image Reconstruction in Diffuse Optical Tomography. Scientific Reports, 2016, 6, 22242.	3.3	15
48	Prefrontal responses to Stroop tasks in subjects with post-traumatic stress disorder assessed by functional near infrared spectroscopy. Scientific Reports, 2016, 6, 30157.	3.3	32
49	Detecting positive surgical margins: utilisation of lightâ€reflectance spectroscopy on <i>ex vivo</i> prostate specimens. BJU International, 2016, 118, 885-889.	2.5	8
50	Wavelet coherence analysis of dynamic cerebral autoregulation in neonatal hypoxic–ischemic encephalopathy. NeuroImage: Clinical, 2016, 11, 124-132.	2.7	94
51	Light Reflectance Spectroscopy to Detect Positive Surgical Margins on Prostate Cancer Specimens. Journal of Urology, 2016, 195, 479-484.	0.4	13
52	The Scalp Confounds Near-Infrared Signal from Rat Brain Following Innocuous and Noxious Stimulation. Brain Sciences, 2015, 5, 387-399.	2.3	0
53	Hemodynamic and Light-Scattering Changes of Rat Spinal Cord and Primary Somatosensory Cortex in Response to Innocuous and Noxious Stimuli. Brain Sciences, 2015, 5, 400-418.	2.3	9
54	Evaluation of cortical plasticity in children with cerebral palsy undergoing constraint-induced movement therapy based on functional near-infrared spectroscopy. Journal of Biomedical Optics, 2015, 20, 046009.	2.6	31

#	Article	IF	CITATIONS
55	Predicting N2pc from anticipatory HbO activity during sustained visuospatial attention: A concurrent fNIRS–ERP study. NeuroImage, 2015, 113, 225-234.	4.2	15
56	Multiregional functional near-infrared spectroscopy reveals globally symmetrical and frequency-specific patterns of superficial interference. Biomedical Optics Express, 2015, 6, 2786.	2.9	31
57	Quantification and normalization of noise variance with sparsity regularization to enhance diffuse optical tomography. Biomedical Optics Express, 2015, 6, 2961.	2.9	6
58	Tutorial on use of intraclass correlation coefficients for assessing intertest reliability and its application in functional near-infrared spectroscopy–based brain imaging. Journal of Biomedical Optics, 2015, 20, 050801.	2.6	59
59	Dynamic functional connectivity revealed by resting-state functional near-infrared spectroscopy. Biomedical Optics Express, 2015, 6, 2337.	2.9	39
60	Pilot examination of functional Near-Infrared spectroscopy (fNIRS) to quantify chemobrain Journal of Clinical Oncology, 2015, 33, e20680-e20680.	1.6	1
61	2D diffuse optical imaging using clustered sparsity. , 2014, , .		1
62	Prostate cancer detection using combined auto-fluorescence and light reflectance spectroscopy: ex vivo study of human prostates. Biomedical Optics Express, 2014, 5, 1512.	2.9	19
63	Atlas-guided volumetric diffuse optical tomography enhanced by generalized linear model analysis to image risk decision-making responses in young adults. Human Brain Mapping, 2014, 35, 4249-4266.	3.6	21
64	An fNIRS investigation of associative recognition in the prefrontal cortex with a rapid event-related design. Journal of Neuroscience Methods, 2014, 235, 308-315.	2.5	37
65	Prefrontal responses to digit span memory phases in patients with post-traumatic stress disorder (PTSD): A functional near infrared spectroscopy study. NeuroImage: Clinical, 2014, 4, 808-819.	2.7	52
66	Depth-compensated diffuse optical tomography enhanced by general linear model analysis and an anatomical atlas of human head. NeuroImage, 2014, 85, 166-180.	4.2	43
67	Hierarchical Clustering Method to Improve Transrectal Ultrasound-guided Diffuse Optical Tomography for Prostate Cancer Imaging. Academic Radiology, 2014, 21, 250-262.	2.5	18
68	Interleaved imaging of cerebral hemodynamics and blood flow index to monitor ischemic stroke and treatment in rat by volumetric diffuse optical tomography. NeuroImage, 2014, 85, 566-582.	4.2	14
69	Investigation of Prefrontal Hemodynamics of PTSD Patients While Performing Stroop Task Using fNIRS. , 2014, , .		2
70	Optical properties of ex-vivo prostate tissues and the design of trans-rectal ultrasound coupled optical probe. , 2014, , .		0
71	A cost-efficient frequency-domain photoacoustic imaging system. American Journal of Physics, 2013, 81, 712-717.	0.7	31
72	A Preliminary Investigation of Human Frontal Cortex Under Noxious Thermal Stimulation Over the Temporomandibular Joint Using Functional Near Infrared Spectroscopy. Journal of Applied Biobehavioral Research, 2013, 18, 134-155.	2.0	4

#	Article	IF	CITATIONS
73	Hierarchical clustering method for improved prostate cancer imaging in diffuse optical tomography. , 2013, , .		1
74	EasyTopo: A toolbox for rapid diffuse optical topography based on a standard template of brain atlas. Proceedings of SPIE, 2013, , .	0.8	10
75	Test-retest assessment of cortical activation induced by repetitive transcranial magnetic stimulation with brain atlas-guided optical topography. Journal of Biomedical Optics, 2012, 17, 116020.	2.6	32
76	Sparsity enhanced spatial resolution and depth localization in diffuse optical tomography. Biomedical Optics Express, 2012, 3, 943.	2.9	52
77	Cerebrovascular responses of the rat brain to noxious stimuli as examined by functional near-infrared whole brain imaging. Journal of Neurophysiology, 2012, 107, 2853-2865.	1.8	6
78	Auto-fluorescence lifetime and light reflectance spectroscopy for breast cancer diagnosis: potential tools for intraoperative margin detection. Biomedical Optics Express, 2012, 3, 1825.	2.9	49
79	Comparison of neural correlates of risk decision making between genders: An exploratory fNIRS study of the Balloon Analogue Risk Task (BART). NeuroImage, 2012, 62, 1896-1911.	4.2	103
80	Embolic middle cerebral artery occlusion model using thrombin and fibrinogen composed clots in rat. Journal of Neuroscience Methods, 2012, 211, 296-304.	2.5	22
81	A globally convergent numerical method for coefficient inverse problems for thermal tomography. Applicable Analysis, 2011, 90, 1573-1594.	1.3	2
82	Quantification of light reflectance spectroscopy and its application: Determination of hemodynamics on the rat spinal cord and brain induced by electrical stimulation. NeuroImage, 2011, 56, 1316-1328.	4.2	16
83	Test–retest assessment of independent component analysis-derived resting-state functional connectivity based on functional near-infrared spectroscopy. NeuroImage, 2011, 55, 607-615.	4.2	87
84	Simultaneous absolute measures of glabrous skin hemodynamic and light-scattering change in response to formalin injection in rats. Neuroscience Letters, 2011, 492, 59-63.	2.1	4
85	Enhanced Functional Brain Imaging by Using Adaptive Filtering and a Depth Compensation Algorithm in Diffuse Optical Tomography. IEEE Transactions on Medical Imaging, 2011, 30, 1239-1251.	8.9	44
86	Resting-state functional connectivity assessed with two diffuse optical tomographic systems. Journal of Biomedical Optics, 2011, 16, 046006.	2.6	45
87	A DUAL-MODALITY OPTICAL BIOPSY APPROACH FOR IN VIVO DETECTION OF PROSTATE CANCER IN RAT MODEL. Journal of Innovative Optical Health Sciences, 2011, 04, 269-277.	1.0	8
88	An effective classification procedure for diagnosis of prostate cancer in near infrared spectra. Expert Systems With Applications, 2010, 37, 3863-3869.	7.6	33
89	Comprehensive investigation of three-dimensional diffuse optical tomography with depth compensation algorithm. Journal of Biomedical Optics, 2010, 15, 046005.	2.6	42
90	A globally convergent numerical method for an inverse elliptic problem of optical tomography. Applicable Analysis, 2010, 89, 861-891.	1.3	13

#	Article	IF	CITATIONS
91	Algorithmic depth compensation improves quantification and noise suppression in functional diffuse optical tomography. Biomedical Optics Express, 2010, 1, 441.	2.9	20
92	Quantification of functional near infrared†spectroscopy to assess cortical reorganization †in children with cerebral palsy. Optics Express, 2010, 18, 25973.	3.4	37
93	Development of a compensation algorithm for accurate depth localization in diffuse optical tomography. Optics Letters, 2010, 35, 429.	3.3	58
94	Investigation of the prefrontal cortex in response to duration-variable anagram tasks using functional near-infrared spectroscopy. Journal of Biomedical Optics, 2009, 14, 054016.	2.6	28
95	A stereotactic near-infrared probe for localization during functional neurosurgical procedures: further experience. Journal of Neurosurgery, 2009, 110, 263-273.	1.6	41
96	Using simultaneous repetitive Transcranial Magnetic Stimulation/functional Near Infrared Spectroscopy (rTMS/fNIRS) to measure brain activation and connectivity. NeuroImage, 2009, 47, 1177-1184.	4.2	61
97	Near infrared and visible spectroscopic measurements to detect changes in light scattering and hemoglobin oxygen saturation from rat spinal cord during peripheral stimulationâ [~] †. NeuroImage, 2008, 40, 217-227.	4.2	12
98	Noninvasive monitoring of estrogen effects against ischemic stroke in rats by near-infrared spectroscopy. Applied Optics, 2007, 46, 8315.	2.1	12
99	Determination of hemoglobin oxygen saturation in rat sciatic nerve by in vivo near infrared spectroscopy. Brain Research, 2006, 1098, 86-93.	2.2	2
100	Tumour oxygen dynamics measured simultaneously by near-infrared spectroscopy and19F magnetic resonance imaging in rats. Physics in Medicine and Biology, 2006, 51, 45-60.	3.0	68
101	Application of Near Infrared Spectroscopy to Study Hot Flashes in Women. , 2006, , .		0
102	Application of Near Infrared Multi-spectral CCD Imager to Determine the Hemodynamic Changes in Prostate Tumor. , 2006, , .		4
103	Acute Effects of Combreatastatin A4 Phosphate on Breast Tumor Hemodynamics Monitored by Near Infrared Spectroscopy. , 2006, , .		1
104	Extinction coefficients of hemoglobin for near-infrared spectroscopy of tissue. IEEE Engineering in Medicine and Biology Magazine, 2005, 24, 118-121.	0.8	64
105	Light scattering from rat nervous system measured intraoperatively by near-infrared reflectance spectroscopy. Journal of Biomedical Optics, 2005, 10, 051405.	2.6	15
106	Investigation of rat breast tumour oxygen consumption by near-infrared spectroscopy. Journal Physics D: Applied Physics, 2005, 38, 2682-2690.	2.8	11
107	Estimated fraction of tumor vascular blood contents sampled by near infrared spectroscopy and ^19F magnetic resonance spectroscopy. Optics Express, 2005, 13, 1724.	3.4	13
108	Investigation of bi-phasic tumor oxygen dynamics induced by hyperoxic gas intervention: A numerical study. Optics Express, 2005, 13, 4465.	3.4	4

#	Article	IF	CITATIONS
109	Determination of reduced scattering coefficient of biological tissue from a needle-like probe. Optics Express, 2005, 13, 4828.	3.4	104
110	Detection of degeneration in rat sciatic nerve by in vivo near infrared spectroscopy. Brain Research Protocols, 2005, 14, 119-125.	1.6	7
111	Effect of Photothermal Therapy on Breast Tumor Vascular Contents: Noninvasive Monitoring by Nearâ€infrared Spectroscopy [¶] . Photochemistry and Photobiology, 2005, 81, 1002-1009.	2.5	5
112	Effect of Photothermal Therapy on Breast Tumor Vascular Contents: Noninvasive Monitoring by Near-infrared Spectroscopy¶. Photochemistry and Photobiology, 2005, 81, 1002.	2.5	19
113	Near-Infrared Spectroscopy and Imaging of Tumor Vascular Oxygenation. Methods in Enzymology, 2004, 386, 349-378.	1.0	24
114	Correlation of NIR spectroscopy with BOLD MR imaging of assessing breast tumor vascular oxygen status. , 2004, , .		2
115	Investigation of breast tumor hemodynamics using tumor vascular phantoms and FEM simulations. , 2004, , .		1
116	Tumor oxygen dynamics measured simultaneously by nearinfrared spectroscopy and 19F MR EPI imaging. , 2004, , .		0
117	Dynamic response of breast tumor oxygenation to hyperoxic respiratory challenge monitored with three oxygen-sensitive parameters. Applied Optics, 2003, 42, 2960.	2.1	44
118	Limited possibility for quantifying mean particle size by logarithmic light-scattering spectroscopy. Applied Optics, 2003, 42, 2968.	2.1	4
119	Look-Ahead Distance of a fiber probe used to assist neurosurgery: Phantom and Monte Carlo study. Optics Express, 2003, 11, 1844.	3.4	38
120	Interplay of tumor vascular oxygenation and tumor pO[sub 2] observed using near-infrared spectroscopy, an oxygen needle electrode, and [sup 19]F MR pO[sub 2] mapping. Journal of Biomedical Optics, 2003, 8, 53.	2.6	70
121	Correlation between total hemoglobin concentration and blood volume of breast tumors measured by NIR spectroscopy and 19F MRS of PFOB. , 2002, , .		0
122	Investigation of tumor oxygen consumption and tumor vascular oxygen dynamics in response to pharmacological interventions by NIRS. , 2002, , .		0
123	Unified analysis of the sensitivities of reflectance and path length to scattering variations in a diffusive medium. Applied Optics, 2001, 40, 1742.	2.1	16
124	Determination of Hemoglobin Oxygen Saturation from Turbid Media Using Reflectance Spectroscopy with Small Source-Detector Separations. Applied Spectroscopy, 2001, 55, 1686-1694.	2.2	21
125	Use of an intracranial near-infrared probe for localization during stereotactic surgery for movement disorders. Journal of Neurosurgery, 2000, 93, 498-505.	1.6	33
126	Noninvasive investigation of blood oxygenation dynamics of tumors by near-infrared spectroscopy. Applied Optics, 2000, 39, 5231.	2.1	114

#	Article	IF	CITATIONS
127	Experimental validation of a backpropagation algorithm for three-dimensional breast tumor localization. IEEE Journal of Selected Topics in Quantum Electronics, 1999, 5, 1049-1057.	2.9	8
128	Reversal of Stem Cellâ€derived Hypertrophic Adipocytes Mediated by Photobiomodulation (1064 nm). Translational Biophotonics, 0, , e202100006.	2.7	0
129	Enhancement of Frequency-Specific Hemodynamic Power and Functional Connectivity by Transcranial Photobiomodulation in Healthy Humans. Frontiers in Neuroscience, 0, 16, .	2.8	6
130	Influence of the Signal-To-Noise Ratio on Variance of Chromophore Concentration Quantification in Broadband Near-Infrared Spectroscopy. Frontiers in Photonics, 0, 3, .	2.4	4